

Nitrogen Fixation by an Arc Plasma at Elevated Pressure to Increase the Energy Efficiency and Production Rate of NO_x Ivan Tsonev,[‡] Colin O'Modhrain,[‡] Annemie Bogaerts, and Yury Gorbanev*Cite This: *ACS Sustainable Chem. Eng.* 2023, 11, 1888–1897

Read Online

ACCESS |



Metrics & More



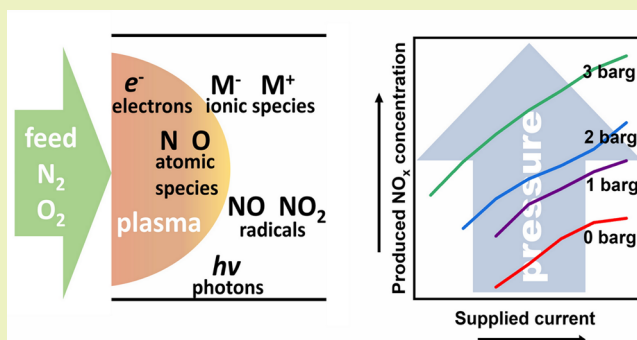
Article Recommendations



Supporting Information

ABSTRACT: Plasma-based nitrogen fixation for fertilizer production is an attractive alternative to the fossil fuel-based industrial processes. However, many factors hinder its applicability, e.g., the commonly observed inverse correlation between energy consumption and production rates or the necessity to enhance the selectivity toward NO_2 , the desired product for a more facile formation of nitrate-based fertilizers. In this work, we investigated the use of a rotating gliding arc plasma for nitrogen fixation at elevated pressures (up to 3 barg), at different feed gas flow rates and composition. Our results demonstrate a dramatic increase in the amount of NO_x produced as a function of increasing pressure, with a record-low EC of 1.8 MJ/(mol N) while yielding a high production rate of 69 g/h and a high selectivity (94%) of NO_2 . We ascribe this improvement to the enhanced thermal Zeldovich mechanism and an increased rate of NO oxidation compared to the back reaction of NO with atomic oxygen, due to the elevated pressure.

KEYWORDS: nitrogen fixation, NO_x plasma, pressure, energy consumption, production rate, rate constant



INTRODUCTION

Nitrogen fixation (NF) is the process of transforming chemically inert atmospheric N_2 into accessible nitrogen and is one of the most important tasks of chemical industry. The process of producing nitrogen-based fertilizers is paramount for ensuring the amount of food required to meet the demands of the increasing world's population. Currently, most nitrogen-based fertilizers are produced by the Haber–Bosch process (HB)—one of the largest industrial chemical processes. However, the large-scale HB is very energy-intensive, consuming 1–2% of global energy annually—primarily in the form of fossil energy carriers.¹ While the most modern iteration of HB reduces CO_2 emissions through utilization and production of a combined urea/ammonium nitrate fertilizer (UAN), the process still releases over 300 Mt of CO_2 per year.² This contributes greatly to the global greenhouse gas emissions (i.e., industrial fossil-fuel usage), adding to the detrimental effects of global warming. HB has been extensively optimized over the century-long period of its existence, leading to a very low energy consumption (EC) for NF into NH_3 (0.5 MJ/(mol N)).³ However, it is efficient only with the currently employed large-scale centralized production sites and requires further distribution via fossil-fuel based transportation (which was not accounted for in the CO_2 production value stated above). The current geopolitical situation and the related fossil energy crisis renders HB unfavorable in the modern-day.

Other, alternative technologies of NF are being actively and extensively researched.

Among such technologies, plasma-based NF is highly attractive. Plasma is a partially or fully ionized gas with collective properties. Besides neutral gas molecules, it also comprises electrons, ions, atoms, excited states, radicals, and photons, creating a highly reactive environment. Plasma-based NF is particularly interesting because it (i) operates at overall much more benign conditions compared to the HB's high temperature and pressure (700–1000 K, 200–400 bar), (ii) has a “turn-key” capability, which enables synergy and integration with renewable resources, (iii) can be decentralized in small-scale plants (removing the need for postproduction transport), and (iv) provides a much higher production rate (PR) than other investigated technologies (e.g., electrochemical NF).⁴

Various pathways of NF by plasma have been studied, ranging from a direct HB alternative of plasma-catalytic N_2 reduction with H_2 ^{5,6} to plasma-electrochemical N_2 reduction and/or oxidation with H_2O , as demonstrated in recent

Received: October 24, 2022

Revised: January 6, 2023

Published: January 23, 2023



Table 1. Overview of Recent Advances in Plasma-Based N₂ Fixation via Oxidation to NO_x and Their Relevant Energy Consumption and Production Rate Values

entry	discharge type	pressure (barg)	N ₂ /O ₂	energy consumption (MJ/(mol N))	total NO _x production rate (g/h)	NO ₂ selectivity (%)	reference
1	pulsed DC spark	0	4:1	0.4	0.3	0	12
2	pulsed AC spark	0	4:1	0.4	<0.1	20	13
3	DC glow	0	4:1	2.8	1.9	5	14
4	microwave (surface wave)	0	1:1	2.0	85.9	71	15
5	three-level coupled rotating electrodes discharge	0	4:1	2.7	0.4	5	16
6	low-current glow-type discharge	0	4:1	3.4	3.0	20	17
7	pulsed gliding arc	0	1:1	4.8	<0.1	40	18
8	rotating gliding arc	0	1:1	2.5	7.0	79	19
9	rotating gliding arc (effusion nozzle)	0	1:1	2.1	7.4	75	20
10	rotating gliding arc (elevated pressure)	3	1:1	1.8	68.9	94	this work

reviews.^{7–9} Presently, the most energy-efficient method of plasma-based NF is via oxidation to nitrogen oxides (NO_x), which can be either used as-is or converted to NH₃ via subsequent catalytic¹⁰ or electrochemical reduction.¹¹

A variety of plasma reactors (and discharge types) have been applied to this purpose, from dielectric barrier discharge (DBD) to thermal arc plasmas.^{3,8} The most recent advances in plasma-based NO_x generation with the lowest reported EC are summarized in Table 1. One of the main difficulties with finding the optimal plasma setup is the reverse correlation between EC and NO_x yield (and PR). An extremely low EC (<0.5 MJ/mol) is often accompanied by a low PR (≤0.1 g/h) (see entries 1 and 2 in Table 1). To our knowledge, the best metrics in terms of low EC and high PR were obtained with the rotating gliding arc (RGA) plasma (entries 8 and 9) and microwave (MW) plasma (entry 4). Despite seeming to be the most viable plasma-based NF option, MW plasmas often require a low-pressure ignition sequence and active cooling. This extra energy is not reflected in the reported EC, resulting in a much higher “plug-to-NO_x” EC, i.e., the EC based on the total amount of energy consumed by the plasma power supply from the mains. In contrast, RGA plasma reactor operation is more facile, but its NO_x EC is somewhat higher when used without additionally designed parts, such as effusion nozzles (entries 8 and 9).

One of the key appeals of plasma processes is their operation at atmospheric pressure, as opposed to high pressures required for HB. However, elevated pressures of several bar can be easily achieved with a simple needle valve, and the created backpressure does not require special feed gas flow equipment outside of standard mass flow controllers (MFCs). In addition, the high gas temperatures observed in arc or MW plasmas (several thousand K) are a consequence of electron acceleration due to the applied electric field and the subsequent transfer of energy to heavier particles through collisions. Thus, in addition to the potential for electronic and vibrational excitation of the plasma species, the plasma is able to reach high gas temperatures without additional external heating.

Fundamental phenomena of high-pressure plasmas in a variety of gases have been extensively studied, both experimentally and theoretically, including high-pressure arc discharges.^{21–23} However, the reports focusing on applications of elevated pressure plasma to gas conversion are scarce. Several works involving CO₂ splitting in DBD reactors at elevated pressure have been carried out,^{24,25} in addition to

hydrocarbons synthesis from syngas using high-pressure arcs.²⁶ The importance of plasmas above atmospheric pressure is also highlighted in the newly published low-temperature plasma roadmap.²⁷ To the best of our knowledge, to date there have been no published works dedicated to studying plasma-based NF into NO_x at elevated pressure.

In this work, we investigated the use of the RGA plasma reactor previously used by our group for NF at atmospheric pressure.^{19,20} We conducted experiments at elevated pressures (1–3 barg, i.e., ca. 2–4 atm), at different feed gas flow rates (4, 8, and 12 Ln/min) and compositions (air, N₂/O₂ 4:1; oxygen-enriched air, N₂/O₂ 1:1). We observed dramatic improvements in NO_x yield, PR, and EC upon rising pressure, as well as a change in the NO_x product distribution with a shift toward NO₂.

EXPERIMENTAL SECTION

The plasma reactor used in this work was similar to described in our previous works.^{19,20} The feed gas flow (N₂/O₂ of 4:1 or 1:1, total flow rate 4, 8, or 12 Ln/min) was supplied using mass flow controllers (MFC, Bronkhorst F-210CV) connected to N₂ and O₂ gas cylinders (both 99.999%, Praxair). The feed gases N₂ and O₂ were mixed using a T-connector, and the mixture was introduced into the RGA plasma reactor (Figure 1). The reactor comprised the main part (consisting

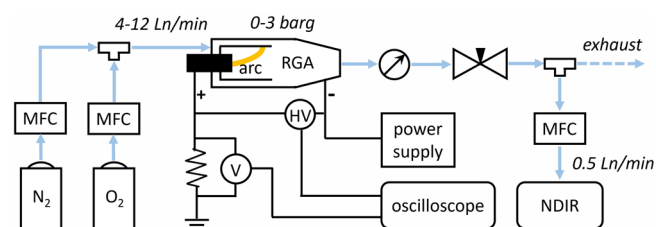


Figure 1. Schematic representation of the RGA plasma setup for NO_x production, with an illustrated high-temperature arc inside the RGA reactor.

of a spark plug and the immediate surroundings) and the long reactor body (stainless steel). The detailed description of the reactor itself is found elsewhere¹⁹ and shown in Figure S1 in the Supporting Information (SI).

The outlet of the plasma reactor was connected to a manometer (Keller LEO2) and a needle valve, which allowed for monitoring and varying the pressure inside the reactor, respectively. Details on the pressure and mass flow rate are found in the SI, section ST1 and Figure S2.

The discharge was driven by a high-voltage current-controlled DC power supply unit (PSU) Technix SR12KV-10KW. The electrical

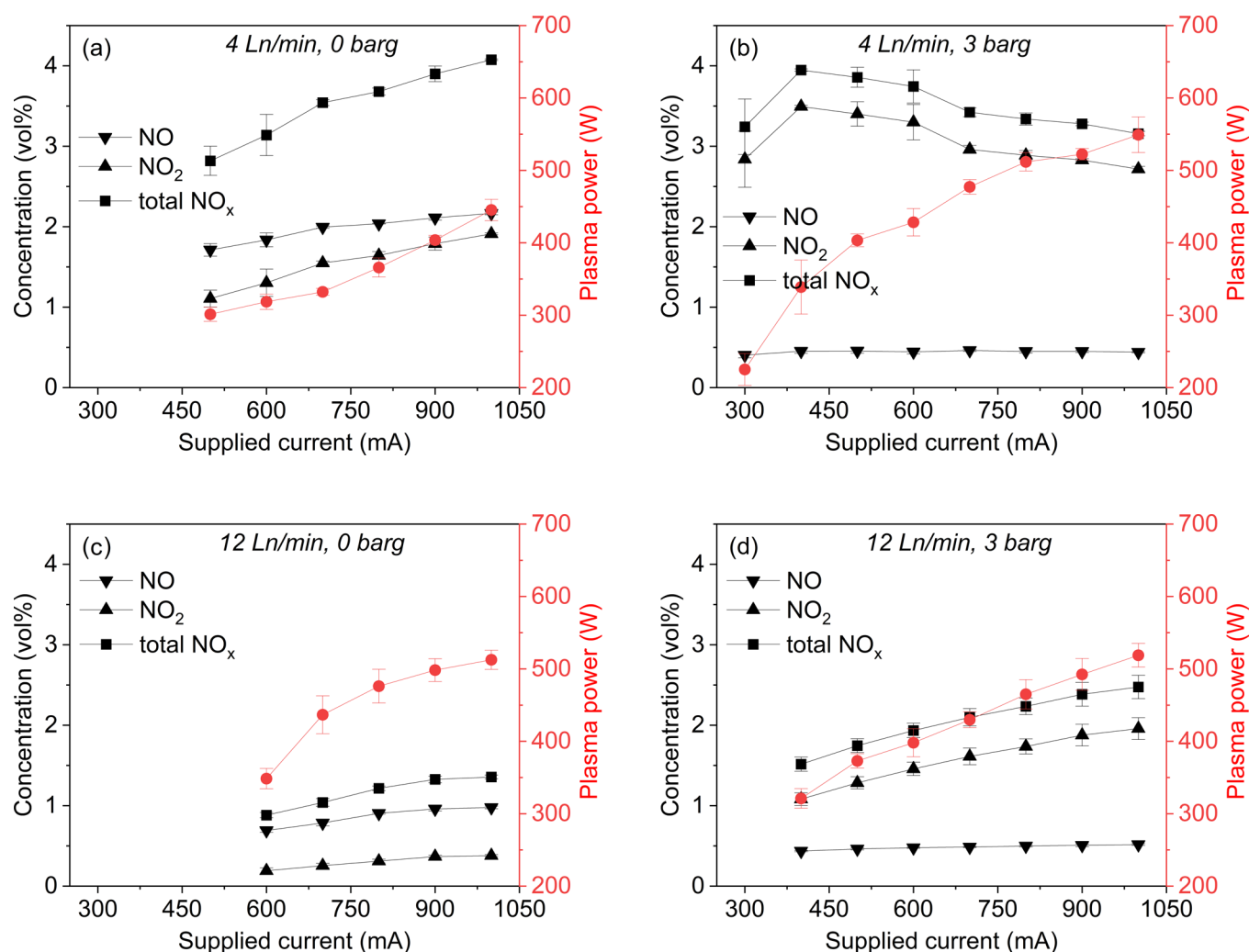


Figure 2. Concentration of produced NO_x and plasma power with N₂/O₂ 4:1, with different gas flow rates, as a function of the PSU current: (a) 4 Ln/min, 0 barg; (b) 4 Ln/min, 3 barg; (c) 12 Ln/min, 0 barg; and (d) 12 Ln/min, 3 barg. The results are presented for conditions that produced the stable takeover discharge mode (see text).

characteristics were monitored with a digital oscilloscope (Keysight InfiniiVision DSOX1102A) using a high voltage probe (Tektronix P6015A). The voltage over a shunt resistor (2 Ω) was measured as shown in Figure 1, to estimate the current values. The reactor was positioned on a wooden surface, and the only path of the current to ground was through the shunt resistor. The sample rates used in the presented data were 10 MSa/s on a 5 ms time scale. In order to determine the accuracy of the data, we varied the sampling rate between 10 MSa/s (5 ms) and 1 MSa/s (50 ms) and observed no significant changes in the average voltage, average current, and the average power.

The total power consumption (defined as the plug power, i.e., the energy used by the PSU) was measured using a three-phase power meter (Chauvin Arnoix MEMO TD80). The temperature of the outer walls of the RGA plasma reactor was measured with an IR thermal imaging camera (Bosch GTC 600 C, -20 to +600 °C, accuracy ±0.1 °C).

The concentration of the produced NO_x in the gas outlet from the RGA reactor was analyzed with a nondispersive infrared (NDIR) sensor (Emerson, Rosemount X-stream enhanced XEGP continuous gas analyzer) as described in section ST2 in the SI.

The calculation of the plasma power, EC, and NO_x PR is detailed in ST3 in the SI.

Each experiment was conducted in triplicate. The error bars represent standard deviations between the obtained values. We note

that in some cases the error bars are too small to be visible on the graphs but are present for every data point.

RESULTS AND DISCUSSION

We investigated the performance of our reactor for two different feed gas ratios: N₂/O₂ of 4:1 and 1:1. Each mixture was examined at feed gas flow rates of 4, 8, and 12 Ln/min. A current-controlled PSU was used, i.e., we were able to vary the current value while the voltage varied in response. At a constant current, the power deposition into the plasma increases upon rising pressure, indicating that the average voltage increases. Under all conditions studied, we observed the formation of NO_x. We report NO_x concentration, plasma power, EC, and PR as a function of the supplied current. We specifically note that we present the data as a function of the PSU-supplied current for clarity and consistency. The values of the plasma-deposited current varied from the PSU-supplied current. The plasma-deposited current values were calculated as shown in ST3 in the SI, and these values were implemented in the calculations of the plasma power and EC.

Production of NO_x from Air (N₂/O₂ mixture 4:1). The results for N₂/O₂ 4:1 at flow rates of 4 and 12 Ln/min are

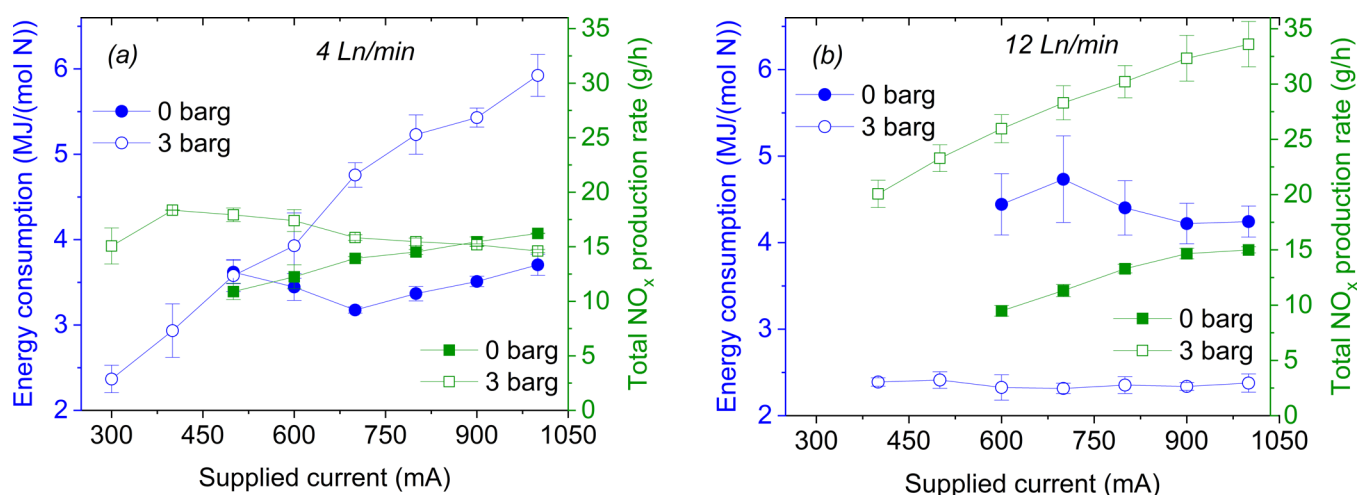


Figure 3. Energy consumption and total NO_x production rate with N₂/O₂ 4:1, at 0 and 3 barg, with (a) 4 Ln/min and (b) 12 Ln/min. The results are presented for conditions that produced the stable takeover discharge mode (see text).

shown in Figures 2a,b and 3a and Figures 2c,d and 3b, respectively.

We observed two distinct modes of plasma operation, characterized as restrike and takeover modes.^{28,29} These two modes occur as a function of increasing current and are typically discriminated by a decreasing level of voltage fluctuations. The restrike mode is characterized by repeated ignition and extinguishing of the arc, resulting in large voltage fluctuations. The takeover mode occurs at higher current, resulting in quasi-regular arc movement and quasi-periodic voltage fluctuations with a lower amplitude compared to the restrike. The differences in the current and voltage waveforms of the two modes are shown in the SI (Figure S3).

In all experiments, we examined only the conditions that allowed the takeover mode. For example, at 0 barg and 4 L/min, this mode of operation could only be achieved at a minimal PSU current of 500 mA (Figure 2a). The restrike mode was avoided because it produces electromagnetic interference, affecting the analytical equipment and presenting potential hazards.

It is generally accepted in plasma-based nitrogen fixation that NO_x production occurs via dissociation of N₂ and O₂ into N and O followed by the Zeldovich reactions, as shown in simplified reactions R1–R6.^{13,30} In general, in plasmas, these reactions can either be thermally or vibrationally promoted, depending on the species present.



First, we studied NO_x production at a 4 Ln/min feed gas flow rate. At 0 barg, a gradual rise of the plasma-deposited power by ca. 1.5 times (from 300 to 445 W), as a consequence of increasing the supplied current (from 500 to 1000 mA) yielded a higher amount of NO_x produced, by a factor of 1.6: from 2.8 to 4.1 vol% (Figure 2a), with the latter corresponding

to the highest PR of 16.2 g/h (Figure 3a). These closely proportional changes of NO_x concentration and power lead to a relatively constant EC, around 3.5 MJ/mol (Figure 3a). It is worth noting that PR is governed by two factors: the total NO_x concentration and the product ratio of NO/NO₂ (see eq SE6 in the SI). In this particular case, the higher plasma-deposited power did not affect the product distribution, which remained within NO/NO₂ of 1.5:1–1:1 (Figure 2a), hence the direct proportionality between total NO_x concentration and PR.

In order to highlight the increased performance at elevated pressures, a comparison of PR and EC must be done at the same power. As mentioned above, we used a current-controlled PSU; hence, we did not have a direct control of power. Therefore, we compare the closest power values at different pressures. At 0 barg and 900 mA PSU-supplied current, the recorded power was ca. 400 W (Figure 2a). These conditions produced 3.9 vol% NO_x at a corresponding PR of 15.5 g/h and EC of 3.5 MJ/(mol N) (Table S1 in the SI shows the comprehensive comparison between different conditions with the closest power values). In contrast, at 2 barg, 400 W of plasma-deposited power was achieved with a lower PSU-supplied current of 600 mA (Figure S4b). This resulted in a higher PR (17.9 g/h) at the same power and a lower EC of 3.3 MJ/(mol N). However, further rising the pressure to 3 barg at 400 W leads to an increase in EC back to 3.5 MJ/mol.

At 3 barg and 4 Ln/min (Figure 2b), the NO_x production did not rise proportionally as a function of the plasma-deposited power. As a result, the EC increased dramatically, from 2.4 MJ/(mol N) at 300 mA to 5.9 MJ/(mol N) at 1 A (Figure 3a). A drop in PR from 18.3 to 14.6 g/h was also observed (Figure 3a).

As mentioned earlier, at a constant current, we observed that the power deposited into the plasma increased as the pressure increased. This suggests that the voltage increased as a function of rising pressure. For example, following the conditions in Figure 2 above, with the flow rate of air of 4 Ln/min and the PSU supplied current value of ca. 500 mA, at 0 barg, the average voltage was 578 V, yielding a power value of 295 W. At 3 barg, the voltage was 736 V, and the power was 383 W. Similarly, the values for 12 Ln/min (at ca. 600 mA) were 572 V and 355 W and 668 V and 414 W at 0 and 3 barg, respectively.

The effect of increasing pressure, however, resulted in a shift of the product distribution, yielding a higher selectivity of NO_2 . The NO/NO_2 ratio changed from around 1:1 at 0 barg to 1:6 at 3 barg. This shift in product ratio is advantageous because higher NO_2 selectivity is beneficial for the nitrate fertilizer-aimed N_2 fixation: NO_2 is more easily absorbed in aqueous washers, thus facilitating the process of NO_3^- accumulation in liquid.^{10,31}

Noteworthy, at elevated pressure, plasma is sustained in the takeover mode at lower currents. For example, with 4 Ln/min, at 0 and 3 barg, we observed the takeover mode at 500 and 300 mA, respectively (Figure 2a,b). It is at these lower currents (300–400 mA) that the lowest EC, at the highest PR, was observed for 4 Ln/min: ca. 2.4 MJ/(mol N) and 16 g/h, respectively, at 3 barg (Figure 3a). The NO_x concentration, EC, and PR for 4 Ln/min, at 1 and 2 barg, are shown in Figures S4 and S5. This effect may be explained by the change in size of the cold gas boundary layer, pushing the attachment point of the arc on the cathode (i.e., where the arc is attached to the reactor wall). Two forces influence the attachment point: the drag force resulting from the gas flow and the electromagnetic force resulting from the movement of charged particles. The increased pressure leads to a higher temperature in the reactor (see the Mechanistic Considerations section below), which in turn reduces the size of the cold gas boundary layer and its effect on the attachment point. The drag force resulting from the gas flow can no longer extend the arc to a point in which restrike can occur, and the more stable takeover mode is achieved.³² Furthermore, the reduced velocity results in a reduced swirl intensity and the arc experiences reduced contracting force. This leads to thickening of the arc column and contributes to a more stabilized arc.

At 0 barg, the results for 8 and 12 Ln/min followed similar trends to one another. The figures relating to the 8 Ln/min case can be found in the SI (Figures S6 and S7). With 12 Ln/min, at 0 barg, the maximal amount of NO_x produced was 1.4 vol% at a deposited power of 515 W (1000 mA supplied current) (Figure 2c). The power increased by 1.6 times (from 350 to 515 W) as a function of the supplied current (from 600 to 1000 mA), while the total NO_x concentration is clearly lower than at 4 Ln/min. This resulted in a higher EC (4.2–4.7 MJ/(mol N)) and lower PR (9.5–15 g/h) for all applied currents at 12 Ln/min and 0 barg (Figure 3b). Compared to 4 Ln/min, the NO/NO_2 ratio shifted toward NO , and constituted 3:1–4:1 at all current values (Figure 2c).

At 3 barg, with 8 and 12 Ln/min, the drop in NO_x concentration and PR (as seen for 4 Ln/min) at higher currents was not observed (Figures S6–S9 and Figure 2d). Instead, the NO_x concentration and power values continued rising proportionally, resulting in a relatively constant EC at all current values (Figure 3b). While the EC remains constant, the higher NO_x concentration yielded a rise in PR from 20 to 34 g/h as a function of increasing current. This higher PR is also linked to the shift in product distribution toward NO_2 : the NO/NO_2 ratio of 1:2 at 400 mA rises to 1:4 at 1000 mA.

The main difference between lower flow rate (4 Ln/min) and higher ones (8 and 12 Ln/min) is that, with higher flow rates at constant power and elevated pressure, both the PR and EC improved more than 2-fold. For example, with 12 Ln/min and 430 W, PR and EC changed from 11 g/h and 4.7 MJ/(mol N) at 0 barg to 28 g/h and 2.3 MJ/(mol N) at 3 barg (see Table S1).

Taken together, our results indicate that elevated pressure (up to 3 barg) can be highly beneficial for the energy and production efficiency values of plasma-based NO_x generation. To date, the unmodified RGA reactor (i.e., without an effusion nozzle²⁰) used in this study was able to produce from air 4.1 vol% NO_x (with 60% NO_2 selectivity) at an EC of 3.0 MJ/(mol N) and PR of ca. 9 g/h.¹⁹ In our experiments, the optimal condition for NO_x production with N_2/O_2 of 4:1 was at 12 Ln/min, 3 barg, and 900 mA PSU current. These conditions yielded 2.4 vol% NO_x (with 80% NO_2), 2.3 MJ/(mol N) EC, and 32 g/h PR (Figures 2d and 3b).

Furthermore, besides the plasma-based EC, we also evaluated the plug-to- NO_x EC, based on the total energy consumption of the power supply, defined by the measured plug power. This is an often overlooked metric in the plasma research community and rarely reported in the literature,³³ although any application-related discussion should include this metric, alongside the commonly used plasma-based EC. For the aforementioned optimal plasma-based EC conditions, the plug-to- NO_x EC was 7 MJ/(mol N). Lower values (5.4 MJ/(mol N)) were obtained at 400 mA PSU, but they corresponded to lower PR and higher plasma-based EC (see Table S2 for all values of plug power and plug-to- NO_x EC).

Mechanistic Considerations. We hypothesize the reasons behind the more efficient production of NO_x at elevated pressure to be (i) elevated gas temperature and (ii) increased rate of NO_2 production, meaning a reduced significance of the back reactions, which lead to loss of NO (back reactions in R3 and R4). Plasmas in which the electron temperature is higher than the gas temperature are characterized as nonequilibrium, while they are in equilibrium when the electron and gas temperatures are equal to each other.³⁴ Naidis et al.³⁵ estimated that at currents around 200 mA, the plasma is in near-local thermodynamic equilibrium (LTE) conditions: both the electric field and the gas temperature predicted by the non-LTE model are in good agreement with the LTE model for currents above 200 mA, indicating that the nonequilibrium effects do not significantly influence the conductivity and the heat balance within the plasma. In our work, we investigate currents >200 mA at elevated pressure; hence, we infer the arc in the RGA reactor is close to thermodynamic equilibrium. In our considerations below, we assume that the electron, vibrational, and gas temperature are in equilibrium and the electron processes do not influence the production of NO directly. While this is likely the case, and the thermal Zeldovich mechanism dominates the overall process, we acknowledge that some part of the observed effect may be due to nonequilibrium phenomena.¹³

Thermodynamic equilibrium composition calculations performed by D'Angola et al.³⁶ as a function of pressure and temperature were used to support our hypothesis. The details of calculating the presented data can be found in the SI (ST4 and Table S3). Figure 4 shows the equilibrium concentration of NO as a function of temperature for different pressures. Below 3000 K, there is no change in the NO concentration for different pressures. Above 3000 K, the concentration reaches a peak and then gradually drops upon increasing temperature. The maximal NO concentration rises from 5 vol% at 0 barg to 6.3 vol% at 3 barg. The maximal concentration peak also shifts toward a higher temperature: from 3500 K at 0 barg to 3800 K at 3 barg. At any given temperature, the NO concentration after the peak (on the right slope) is higher at elevated pressures.

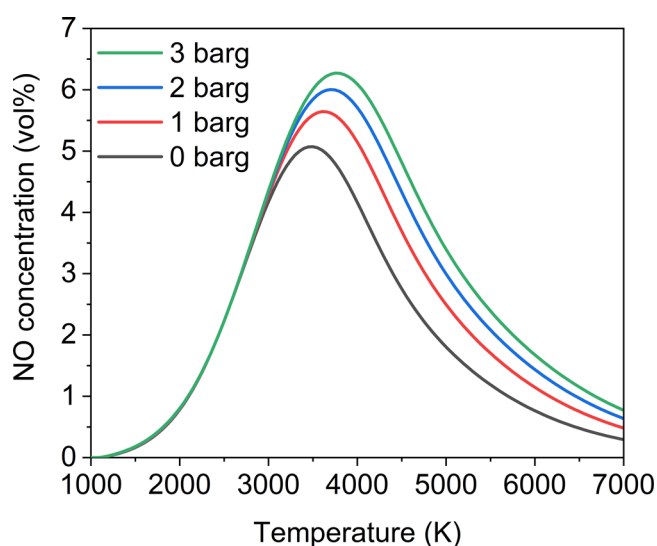


Figure 4. Equilibrium concentration of NO as a function of temperature at different pressures (0–3 barg).

With increasing pressure, we experimentally observe a higher plasma-deposited power and a lower flow velocity (due to the constant mass flow rate). This increased power and higher residence time (i.e., lower velocity) both lead to higher temperatures inside the plasma arc, which in turn lead to higher concentrations of NO as a function of pressure. We note that the concentration of NO discussed here is the NO produced by the plasma and not the final concentration of NO measured downstream, because this plasma-produced NO is further oxidized into NO_2 (see below).

Figure 4 also suggests that the NO concentration can drop when the temperature exceeds the optimal value at the specified pressure, as seen on the right slope, after the peak value. We believe this effect was observed in our experimental results, specifically at 4 Ln/min and 2 and 3 barg (Figure S4 and Figure 2b). At 3 barg, the initial rise of the downstream NO_x concentration from 3.2 to 3.9 vol% is followed by a drop back to 3.2 vol%. This drop in the concentration coincides with the condition with the longest residence time and the highest power. This leads to exceeding the optimal temperature, heating of the plasma beyond 3800 K, and hence lower concentration of the plasma-produced NO. Although the temperature could not be monitored directly, we measured the temperature of the outer walls with an IR camera. At 4 Ln/min, the temperature values recorded were 500, 540, and 580 °C at 0, 1, and 2 barg, respectively. The temperature recorded at 3 barg was >600 °C (an exact measurement could not be taken due to the camera limits). This provides evidence for the temperature increase inside the reactor at elevated pressures. We note, however, that these results cannot be used to directly estimate the temperature inside the reactor and are used qualitatively, exclusively to confirm the rising trend of temperature as a function of rising pressure.

It is important to note that the equilibrium composition cannot explain by itself the high concentrations measured at the outlet of the reactor. The recombination reactions along the gradual temperature drop in the reactor after the plasma partly destroy the created NO coming from the active plasma zone via the back reactions (see R3 and R4).²⁰ This is also seen in our experimental results, where the maximal NO_x concentration obtained was 4.2 vol% at 4 Ln/min and 1 barg

(Figure S4a), while the maximal theoretical equilibrium concentration is 5.6 vol% at 1 barg (Figure 4). We believe that the higher pressure benefits the NO production by limiting the pressure-independent rate coefficient of the recombination reaction (back reaction of R4) and by increasing the pressure-dependent rate coefficient of the oxidation reaction (R5). In Figure 5, the dependence of the

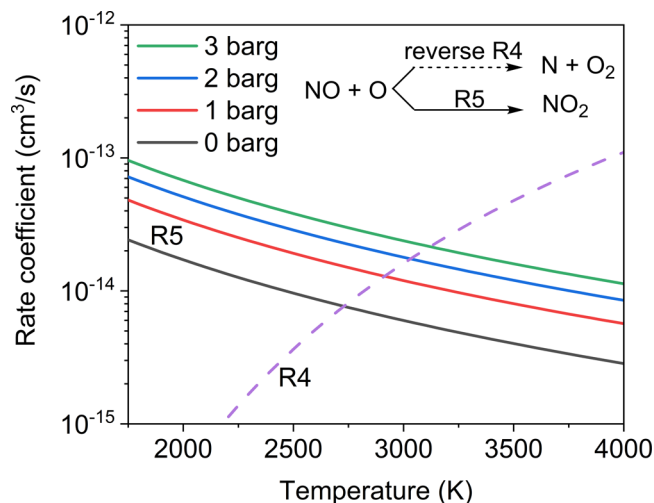


Figure 5. Rate coefficients of the pressure-independent back reaction of R4 and the pressure-dependent forward reaction of R5 as a function of temperature.

reaction rate coefficients for the back reaction of R4 and forward reaction of R5 are compared as a function of temperature for different pressures. The values were taken from Baulch et al.,³⁷ and details about the pressure dependence of R5 can be found in the SI (ST5).

In the low-temperature region (<2500 K), the oxidation of NO to NO_2 will be dominant (R5), while in the high-temperature region (>3000 K), the back reaction of R4 dominates. At 0 barg, the rate constant of the reaction between NO and O (back reaction R4) is equal to the oxidation rate constant at 2700 K, while at 3 barg, this intersection occurs at 3100 K. This suggests that, in our experiments, the temperature in the postplasma compartment of the reactor is below 3100 K, where reaction R5 and the back reaction of R4 occur. The RGA reactor operates without an active quenching system, which means the temperature drop inside the reactor after the plasma is gradual because the energy is primarily lost due to heat transfer with the walls. Following this, with increasing pressure, more NO is oxidized into NO_2 along the temperature gradient due to R5. Although we believe this to be the main mechanism behind increased NO_x production, it cannot be conclusively proven using our current experimental setup.

In all of the experiments performed under elevated pressure, we observe significant NO_2 formation (i.e., high NO_2 selectivity), which could be explained by other oxidation reactions. Specifically, reaction R6 could be responsible for the oxidation of NO in the even lower temperature compartment of the reactor, close to the exhaust,¹⁸ because R6 is reported within 273–600 K.³⁷ Future work involving a computational fluid dynamics model is required to evaluate this mechanism.

Production of NO_x from Oxygen-Enriched Air (N_2/O_2 mixture of 1:1). Literature reports, including our previous

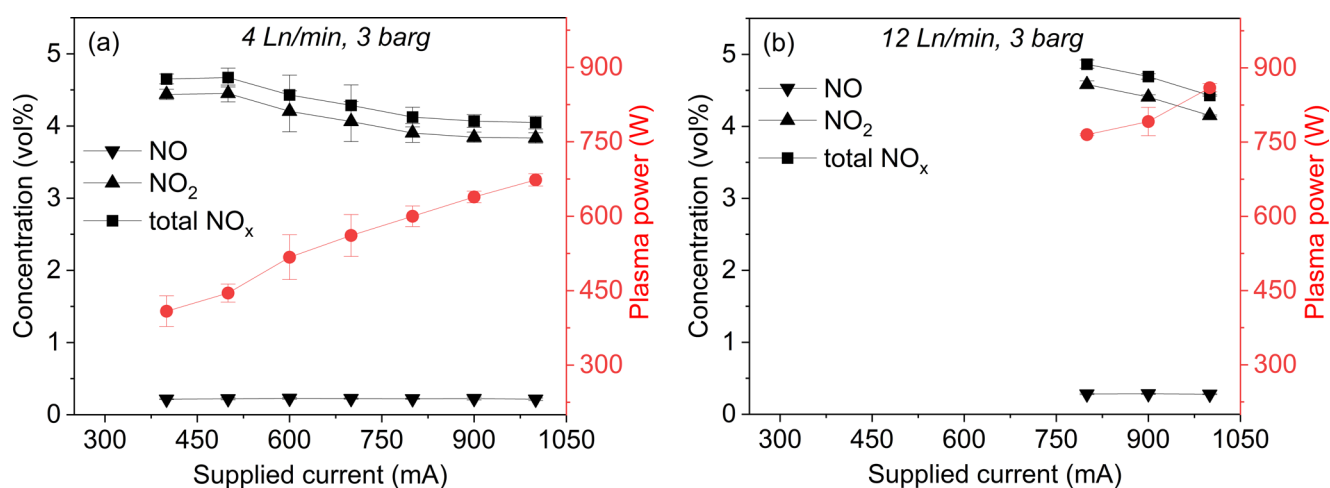


Figure 6. Concentration of produced NO_x and plasma power with N₂/O₂ 1:1, 3 barg, with (a) 4 Ln/min and (b) 12 Ln/min as a function of the current supplied by the PSU. The results are presented for conditions that produced the stable takeover discharge mode (see text).

works with the RGA plasma reactor, show that the lowest EC is achieved with the feed gas N₂/O₂ ratio of 1:1 (e.g., entries 4, 7–10 in Table 1). Obtaining such mixtures is possible for example, via pressure swing adsorption technology, and the evident increase in efficiency presents a clear interest for industrial applications.^{15,19,38} We investigated the performance of our plasma system at 4–12 Ln/min, 0–3 barg, with the N₂/O₂ feed gas ratio of 1:1.

Interestingly, the higher oxygen content in the feed gas resulted in a less stable discharge, only enabling the takeover mode at higher PSU supplied currents. This was most apparent at 12 Ln/min, where even at 3 barg, the plasma could only be sustained at a supplied current above 800 mA (Figure 6b). To our knowledge, the fundamental aspects of the attachment mechanisms in low current oxygen-enriched arcs have not been investigated in the literature. A separate fundamental investigation of this effect is needed in order to explain the instability of the arc.

With 4 Ln/min at 0 barg, the trends of NO_x concentration, EC and PR resembled those observed with the 4:1 ratio (see Figures S10 and S11). The proportional increase in power and NO_x concentration resulted in EC remaining relatively constant (around 4 MJ/(mol N)) as a function of the current. However, the drop in NO_x concentration at high current values started already at 1 barg (Figure S10b) and not at 2 barg, as was the case for 4 Ln/min with the 4:1 N₂/O₂ ratio (Figure S4b). This indicates that already at these conditions we pass the optimal temperature giving rise to the peak production of NO (similar to that in Figure 4 for N₂/O₂ 4:1). Another important difference is that higher O₂ content of the feed gas results in a higher plasma-deposited power for the same current and pressure. We speculate that this higher power results in higher temperature. Although equilibrium compositions of N₂/O₂ mixtures are semiquantitatively described in the literature,^{36,39} the quantitative data is not readily available. However, Ghorui et al. showed that the variation of the gas composition as a function of temperature for the 1:1 N₂/O₂ ratio follows a similar trend to that of 4:1.³⁹ Therefore, we believe the explanations given in the previous section are applicable here, albeit we do not know at which temperature the maximal NO concentration is achieved. Further investigation into the nature of this process would require a detailed chemical kinetic model, which was outside the scope of this

work. At 3 barg and 4 Ln/min, the NO_x production is further limited, giving a dramatic increase in EC (from 3.0 to 5.7 MJ/(mol N)) upon rising current from 400 to 1000 mA (Figure 7), similarly to the N₂/O₂ 4:1 case.

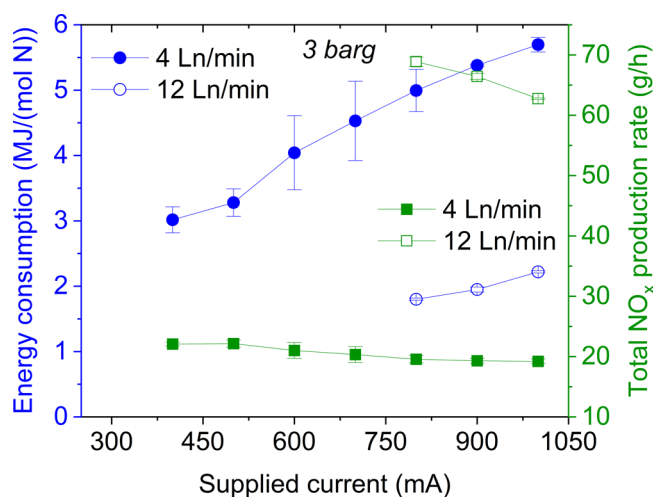


Figure 7. Energy consumption and total NO_x production rate with N₂/O₂ 1:1, 3 barg, and 4 and 12 Ln/min. The results are presented for conditions that produced the stable takeover discharge mode (see text).

With 4 Ln/min, at the near constant power of 440 W, the EC as a function of pressure first decreased (from 4.0 to 3.1 MJ/(mol N), between 0 and 2 barg) and then slightly increased (to 3.3 MJ/(mol N) at 3 barg), while the PR increased (see Table S1), in line with the 4:1 case.

With 8 Ln/min and the N₂/O₂ ratio of 1:1, the trends are once again similar to the 4:1 ratio (Figures S12 and S13). However, with 12 Ln/min, a higher current leads to a lower NO_x concentration (and PR) at all studied pressures (Figures 6b and 7; see also Figures S14 and S15). This results in EC rising from 1.8 to 2.2 MJ/(mol N) (Figure 7). Nonetheless, the performance still improves upon the values obtained at 4 Ln/min, reaching an EC as low as 1.8 MJ/(mol N) with a corresponding PR of 69 g/h at a power of 860 W (supplied current of 800 mA), with the NO/NO₂ ratio of 1:21. Importantly, the NO₂ selectivity was much higher with the

N_2/O_2 ratio of 1:1 than with 4:1, under all investigated conditions, likely due to the increased amount of oxygen available for oxidation. Moreover, at 3 barg, the NO_2 selectivity was relatively independent of the gas flow rate in all experiments. This further demonstrates the advantage of using an oxygen-enriched air mixture for the purpose of plasma-based NF.

The most promising results were obtained at 12 Ln/min and 3 barg—similar to the 4:1 ratio of N_2/O_2 . For this 1:1 case, we were able to generate 4.9 vol% NO_x (almost exclusively NO_2) (Figure 6b), with an EC of merely 1.8 MJ/(mol N) at a high production rate of 69 g/h (Figure 7). At close power values, this corresponds to a rise in PR and a reduction in EC by a factor of 2.3 and 1.8, respectively, compared to those at 0 barg. Furthermore, the corresponding plug-to- NO_x EC was as low as 3.7 MJ/(mol N). This is up to 2 orders of magnitude lower than other competing plasma-based NF technologies, e.g., reported recently by Attri et al.³³ Additional comparison of this value with the literature is difficult due to the common lack of the plug-to- NO_x EC reporting.

CONCLUSIONS

We studied the production of NO_x in an RGA plasma reactor as a function of the supplied current, feed gas flow rate, and ratio at elevated pressure (0–3 barg). At the N_2/O_2 ratio of 4:1 (mimicking dry air) and a feed gas flow rate of 4 Ln/min, we observed an initial improvement of process performance as a function of pressure, i.e., at a power of ca. 400 W, increasing the pressure from 0 to 2 barg led to ca. 15% higher PR and 6% lower EC. Further increasing the pressure to 3 barg however yielded lower NO_x concentration, which was attributed to surpassing the thermal equilibrium peak of NO production. At higher flow rates (8 and 12 Ln/min), we believe we did not surpass the optimal condition for the production of NO, which resulted in an improvement as a function of pressure. At 12 Ln/min, we observed a rise in PR and a drop in EC by factors of 2.5 and 2, respectively, between 0 and 3 barg at a near constant power of 440 W.

We attribute the improvement of EC and PR upon rising pressure to the synergetic effect between the higher equilibrium NO concentration and the oxidation of NO by O to NO_2 . We believe that this oxidation limits the recombination of NO with O (into N and O_2), thus providing a higher NO_x concentration extracted from the postplasma compartment of the reactor.

The high selectivity toward NO_2 , which is beneficial for effective utilization of fixated nitrogen, is also a result of elevated pressure in all three temperature regions of the plasma reactor. Besides favoring the oxidation of NO (formed in the plasma arc, i.e., the highest temperature) with O into NO_2 in the colder postplasma region, higher pressure also increases the rate of NO oxidation by O_2 in the reactor compartment remote from plasma, with temperatures reaching several hundred degrees.

Under optimized conditions (N_2/O_2 ratio of 1:1, with 12 Ln/min, 3 barg, PSU current of 800 mA) our obtained EC of 1.8 MJ/(mol N) is, to our knowledge, the lowest value of plasma-based EC for NO_x generation with a high production rate (>50 g/h) reported to-date in the literature. Furthermore, the total energy efficiency of the process, defined by the plug-to- NO_x EC, is merely 3.7 MJ/(mol N) in our system.

Our work identifies pressure as an important parameter to enhance the plasma NF performance, which is often

overlooked by researchers. In general, plasma operation at slightly elevated pressures does not require equipment any different than that used at atmospheric pressure but improves the process, thus making plasma NF an even more appealing auxiliary technology to the industrial counterparts.

ASSOCIATED CONTENT

Supporting Information

The Supporting Information is available free of charge at <https://pubs.acs.org/doi/10.1021/acssuschemeng.2c06357>.

Figures of detailed scheme of the RGA plasma reactor, schematic representation of the experiments on the MFC flow rate assessment, and voltage as a function of time for the restrike and takeover mode, concentration of produced NO_x and plasma power, and energy consumption and total NO_x production rate, discussions of pressure and mass flow rates, analysis of the plasma reactor outlet for NO_x , calculation of plasma power, energy consumption and production rate values, calculation of equilibrium NO concentration, and calculation of the pressure-dependent rate coefficient RS, and tables of comparison of production rate and plasma-based energy consumption at constant flow rate and power for different pressures and N_2/O_2 ratios, measured values of power consumed by the PSU and the plug-to- NO_x energy consumption for different experimental conditions, and constants for determining the pressure-dependent concentration of NO (PDF)

AUTHOR INFORMATION

Corresponding Author

Yury Gorbanev – Research Group PLASMANT, Department of Chemistry, University of Antwerp, 2610 Wilrijk, Belgium; orcid.org/0000-0002-8059-4464; Phone: +32(0) 32652343; Email: yury.gorbanev@uantwerpen.be

Authors

Ivan Tsonev – Research Group PLASMANT, Department of Chemistry, University of Antwerp, 2610 Wilrijk, Belgium

Colin O'Modhrain – Research Group PLASMANT, Department of Chemistry, University of Antwerp, 2610 Wilrijk, Belgium; orcid.org/0000-0002-0562-4408

Annamie Bogaerts – Research Group PLASMANT, Department of Chemistry, University of Antwerp, 2610 Wilrijk, Belgium; orcid.org/0000-0001-9875-6460

Complete contact information is available at:

<https://pubs.acs.org/doi/10.1021/acssuschemeng.2c06357>

Author Contributions

[‡]I.T. and C.O. contributed equally. The manuscript was written through contributions of all authors. All authors have given approval to the final version of the manuscript.

Funding

This research was financially supported by the European Union's Horizon 2020 research and innovation program (grant No. 965546) and the Fund for Scientific Research (FWO) Flanders Bio-economy project (grant No. G0G2322N), funded by the European Union – NextGenerationEU.

Notes

The authors declare no competing financial interest.

ACKNOWLEDGMENTS

The authors would like to thank Hamid Ahmadi Eshtehardi (PLASMANT) for his help with the schematics of the RGA reactor.

ABBREVIATIONS USED

NF, nitrogen fixation; HB, Haber–Bosch process process; DBD, dielectric barrier discharge; RGA, rotating gliding arc; MW, microwave; MFC, mass flow controller; Ln, normal liters; PSU, power supply unit; NDIR, nondispersive infrared (spectroscopy); EC, energy consumption; PR, production rate; IR, infrared; LTE, local thermodynamic equilibrium

REFERENCES

- (1) Smith, C.; Hill, A. K.; Torrente-Murciano, L. Current and future role of Haber–Bosch ammonia in a carbon-free energy landscape. *Energy Environ. Sci.* **2020**, *13* (2), 331–344.
- (2) International Fertilizer Industry Association. Fertilizers, climate change and enhancing agricultural productivity sustainably. https://www.fertilizer.org//images/Library_Downloads/2009_climate_change_brief.pdf (accessed 2022-10-24).
- (3) Rouwenhorst, K. H. R.; Jardali, F.; Bogaerts, A.; Lefferts, L. From the Birkeland-Eyde process towards energy-efficient plasma-based NO_x synthesis: a techno-economic analysis. *Energy Environ. Sci.* **2021**, *14* (5), 2520–2534.
- (4) Kyriakou, V.; Garagounis, I.; Vasileiou, E.; Vourros, A.; Stoukides, M. Progress in the Electrochemical Synthesis of Ammonia. *Catal. Today* **2017**, *286*, 2–13.
- (5) Hong, J.; Prawer, S.; Murphy, A. B. Plasma Catalysis as an Alternative Route for Ammonia Production: Status, Mechanisms, and Prospects for Progress. *ACS Sustain. Chem. Eng.* **2018**, *6* (1), 15–31.
- (6) Gorbanev, Y.; Engelmann, Y.; van't Veer, K.; Vlasov, E.; Ndayirinde, C.; Yi, Y.; Bals, S.; Bogaerts, A. Al₂O₃-Supported Transition Metals for Plasma-Catalytic NH₃ Synthesis in a DBD Plasma: Metal Activity and Insights into Mechanisms. *Catalysts* **2021**, *11* (10), 1230.
- (7) Chen, H.; Yuan, D.; Wu, A.; Lin, X.; Li, X. Review of low-temperature plasma nitrogen fixation technology. *Waste Dispos. Sustain. Energy* **2021**, *3* (3), 201–217.
- (8) Winter, L. R.; Chen, J. G. N₂ Fixation by Plasma-Activated Processes. *Joule* **2021**, *5* (2), 300–315.
- (9) Rouwenhorst, K. H. R.; Engelmann, Y.; van't Veer, K.; Postma, R. S.; Bogaerts, A.; Lefferts, L. Plasma-driven catalysis: green ammonia synthesis with intermittent electricity. *Green Chem.* **2020**, *22* (19), 6258–6287.
- (10) Hollevoet, L.; Vervloessem, E.; Gorbanev, Y.; Nikiforov, A.; De Geyter, N.; Bogaerts, A.; Martens, J. A. Energy-Efficient Small-Scale Ammonia Synthesis Process with Plasma-Enabled Nitrogen Oxidation and Catalytic Reduction of Adsorbed NO_x. *ChemSusChem* **2022**, *15* (10), e202102526.
- (11) Li, L.; Tang, C.; Cui, X.; Zheng, Y.; Wang, X.; Xu, H.; Zhang, S.; Shao, T.; Davey, K.; Qiao, S. Z. Efficient Nitrogen Fixation to Ammonia through Integration of Plasma Oxidation with Electrocatalytic Reduction. *Angew. Chem., Int. Ed.* **2021**, *60* (25), 14131–14137.
- (12) Britun, N.; Gamaleev, V.; Hori, M. Evidence of near-the-limit energy cost NO formation in atmospheric spark discharge. *Plasma Sources Sci. Technol.* **2021**, *30* (8), 08LT02.
- (13) Vervloessem, E.; Gorbanev, Y.; Nikiforov, A.; De Geyter, N.; Bogaerts, A. Sustainable NO_x production from air in pulsed plasma: elucidating the chemistry behind the low energy consumption. *Green Chem.* **2022**, *24* (2), 916–929.
- (14) Pei, X.; Gidon, D.; Graves, D. B. Specific energy cost for nitrogen fixation as NO_x using DC glow discharge in air. *J. Phys. D: Appl. Phys.* **2020**, *53* (4), 044002.
- (15) Kelly, S.; Bogaerts, A. Nitrogen fixation in an electrode-free microwave plasma. *Joule* **2021**, *5* (11), 3006–3030.
- (16) Lei, X.; Cheng, H.; Nie, L.; Lu, X. Nitrogen Fixation as NO_x Enabled by a Three-Level Coupled Rotating Electrodes Air Plasma at Atmospheric Pressure. *Plasma Chem. Plasma Process.* **2022**, *42* (1), 211–227.
- (17) Korolev, Y. D.; Frants, O. B.; Landl, N. V.; Suslov, A. I. Low-Current Plasmatron as a Source of Nitrogen Oxide Molecules. *IEEE Trans. Plasma Sci.* **2012**, *40* (11), 2837–2842.
- (18) Patil, B. S.; Peeters, F. J. J.; van Rooij, G. J.; Medrano, J. A.; Gallucci, F.; Lang, J.; Wang, Q.; Hessel, V. Plasma assisted nitrogen oxide production from air: Using pulsed powered gliding arc reactor for a containerized plant. *AIChE J.* **2018**, *64* (2), 526–537.
- (19) Jardali, F.; Van Alphen, S.; Creel, J.; Ahmadi Eshtehardi, H.; Axelsson, M.; Ingels, R.; Snyders, R.; Bogaerts, A. NO_x production in a rotating gliding arc plasma: potential avenue for sustainable nitrogen fixation. *Green Chem.* **2021**, *23* (4), 1748–1757.
- (20) Van Alphen, S.; Ahmadi Eshtehardi, H.; O'Modhrain, C.; Bogaerts, J.; Van Poyer, H.; Creel, J.; Delplancke, M.-P.; Snyders, R.; Bogaerts, A. Effusion nozzle for energy-efficient NO_x production in a rotating gliding arc plasma reactor. *Chem. Eng. J.* **2022**, *443*, 136529.
- (21) Benilov, M. S. Understanding and modelling plasma–electrode interaction in high-pressure arc discharges: a review. *J. Phys. D: Appl. Phys.* **2008**, *41* (14), 144001.
- (22) Fulcheri, L.; Rohani, V.; Fabry, F.; Traisnel, N. Experimental electrical characterization of a low-current tip–tip arc discharge in helium atmosphere at very high pressure. *Plasma Sources Sci. Technol.* **2010**, *19* (4), 045010.
- (23) Gueye, P.; Cressault, Y.; Rohani, V.; Fulcheri, L. MHD modeling of rotating arc under restrike mode in 'Kvaerner-type' torch: II. Dynamics and stability at 20 bar pressure. *J. Phys. D: Appl. Phys.* **2019**, *52* (14), 145202.
- (24) Eliasson, B.; Kogelschatz, U.; Xue, B.; Zhou, L.-M. Hydrogenation of Carbon Dioxide to Methanol with a Discharge-Activated Catalyst. *Ind. Eng. Chem. Res.* **1998**, *37* (8), 3350–3357.
- (25) Uytendhouwen, Y.; Bal, K. M.; Michielsen, I.; Neyts, E. C.; Meynen, V.; Cool, P.; Bogaerts, A. How process parameters and packing materials tune chemical equilibrium and kinetics in plasma-based CO₂ conversion. *Chem. Eng. J.* **2019**, *372*, 1253–1264.
- (26) Iwarere, S.; Rohani, V.; Ramjugernath, D.; Fabry, F.; Fulcheri, L. Hydrocarbons synthesis from syngas by very high pressure plasma. *Chem. Eng. J.* **2014**, *241*, 1–8.
- (27) Adamovich, I.; Agarwal, S.; Ahedo, E.; Alves, L. L.; Baalrud, S.; Babaeva, N.; Bogaerts, A.; Bourdon, A.; Bruggeman, P. J.; Canal, C.; Choi, E. H.; Coulombe, S.; Donkó, Z.; Graves, D. B.; Hamaguchi, S.; Hegemann, D.; Hori, M.; Kim, H.-H.; Kroesen, G. M. W.; Kushner, M. J.; Laricchiuta, A.; Li, X.; Magin, T. E.; Mededovic Thagard, S.; Miller, V.; Murphy, A. B.; Oehrlein, G. S.; Puac, N.; Sankaran, R. M.; Samukawa, S.; Shiratani, M.; Šimek, M.; Tarasenko, N.; Terashima, K.; Thomas, E., Jr; Trieschmann, J.; Tsikata, S.; Turner, M. M.; van der Walt, I. J.; van de Sanden, M. C. M.; von Woedtke, T. The 2022 Plasma Roadmap: low temperature plasma science and technology. *J. Phys. D: Appl. Phys.* **2022**, *55* (37), 373001.
- (28) Wutzke, S. A.; Pfender, E.; Eckert, E. R. G. Study of electric arc behavior with superimposed flow. *AIAA J.* **1967**, *5* (4), 707–713.
- (29) Trelles, J. P.; Pfender, E.; Heberlein, J. Multiscale Finite Element Modeling of Arc Dynamics in a DC Plasma Torch. *Plasma Chem. Plasma Process.* **2006**, *26* (6), 557–575.
- (30) Bian, W.; Song, X.; Shi, J.; Yin, X. Nitrogen fixed into HNO₃ by pulsed high voltage discharge. *J. Electrostat.* **2012**, *70* (3), 317–326.
- (31) Pei, X.; Gidon, D.; Yang, Y.-J.; Xiong, Z.; Graves, D. B. Reducing energy cost of NO production in air plasmas. *Chem. Eng. J.* **2019**, *362*, 217–228.
- (32) Noguès, E.; Fauchais, P.; Vardelle, M.; Granger, P. Relation Between the Arc-Root Fluctuations, the Cold Boundary Layer Thickness and the Particle Thermal Treatment. *J. Therm. Spray Technol.* **2007**, *16* (5–6), 919–926.
- (33) Attri, P.; Koga, K.; Okumura, T.; Takeuchi, N.; Shiratani, M. Green route for ammonium nitrate synthesis: fertilizer for plant growth enhancement. *RSC Adv.* **2021**, *11* (46), 28521–28529.

- (34) Burm, K. T. A. L. Plasma: The Fourth State of Matter. *Plasma Chem. Plasma Process.* **2012**, *32* (2), 401–407.
- (35) Naidis, G. V. Simulation of convection-stabilized low-current glow and arc discharges in atmospheric-pressure air. *Plasma Sources Sci. Technol.* **2007**, *16* (2), 297–303.
- (36) D'Angola, A.; Colonna, G.; Gorse, C.; Capitelli, M. Thermodynamic and transport properties in equilibrium air plasmas in a wide pressure and temperature range. *Eur. Phys. J. D* **2008**, *46* (1), 129–150.
- (37) Baulch, D. L.; Bowman, C. T.; Cobos, C. J.; Cox, R. A.; Just, T.; Kerr, J. A.; Pilling, M. J.; Stocker, D.; Troe, J.; Tsang, W.; Walker, R. W.; Warnatz, J. Evaluated Kinetic Data for Combustion Modeling: Supplement II. *J. Phys. Chem. Ref. Data* **2005**, *34* (3), 757–1397.
- (38) Ingels, R. US patent US20210402362A1, 2021.
- (39) Ghorui, S.; Heberlein, J. V. R.; Pfender, E. Thermodynamic and Transport Properties of Two-Temperature Nitrogen-Oxygen Plasma. *Plasma Chem. Plasma Process.* **2008**, *28* (4), 553–582.

Recommended by ACS

Origin of Ammonia Selective Oxidation Activity of SmMn₂O₅ Mullite: A First-Principles-Based Microkinetic Study

Xi Chen, Bin Shan, *et al.*

DECEMBER 20, 2022
ACS APPLIED MATERIALS & INTERFACES

READ 

Ionic Liquid-Assisted Selective Extraction and Partitioning of Biomolecules from Macroalgae

Edgar Suarez Garcia, Michel H. M. Eppink, *et al.*

JANUARY 24, 2023
ACS SUSTAINABLE CHEMISTRY & ENGINEERING

READ 

Porous Silicon Nanocarriers Boost the Immunomodulation of Mitochondria-Targeted Bovine Serum Albumins on Macrophage Polarization

Jialiang Li, Bing Xia, *et al.*

JANUARY 04, 2023
ACS NANO

READ 

Speciation of Oxygen Functional Groups on the Carbon Support Controls the Electrocatalytic Activity of Cobalt Oxide Nanoparticles in the Oxygen Evolution Reaction

Aleksander Ejsmont, Paweł Stelmachowski, *et al.*

JANUARY 19, 2023
ACS APPLIED MATERIALS & INTERFACES

READ 

Get More Suggestions >